Available online at www.sciencedirect.com
ScienceDirect
Trans. Nonferrous Met. Soc. China 19(2009) 635−641
Transactions of Nonferrous Metals Society of China
www.tnmsc.cn

Synthesis of $LiNi_{1/3}Co_{1/3}Mn_{1/3}O_2$ cathode material via oxalate precursor

ZHANG Chuan-fu(张传福), YANG Ping(杨 平), DAI Xi(戴 曦),
XIONG Xuan(熊 宣), ZHAN Jing(湛 菁), ZHANG Yin-liang(张银亮)

School of Metallurgical Science and Engineering, Central South University, Changsha 410083, China

Received 25 June 2008; accepted 11 December 2008

Abstract: Using oxalic acid and stoichiometrically mixed solution of $NiCl_2$, $CoCl_2$, and $MnCl_2$ as starting materials, the triple oxalate precursor of nickel, cobalt, and manganese was synthesized by liquid-phase co-precipitation method. And then the $LiNi_{1/3}Co_{1/3}Mn_{1/3}O_2$ cathode materials for Li-ion battery were prepared from the precursor and $LiOH·H_2O$ by solid-state reaction. The precursor and $LiNi_{1/3}Co_{1/3}Mn_{1/3}O_2$ were characterized by chemical analysis, XRD, EDX, SEM and TG-DTA. The results show that the composition of precursor is $Ni_{1/3}Co_{1/3}Mn_{1/3}C_2O_4·2H_2O$. The product $LiNi_{1/3}Co_{1/3}Mn_{1/3}O_2$, in which nickel, cobalt and manganese are uniformly distributed, is well crystallized with a-$NaFeO_2$ layered structure. Sintering temperature has a remarkable influence on the electrochemical performance of obtained samples. $LiNi_{1/3}Co_{1/3}Mn_{1/3}O_2$ synthesized at 900 ℃ has the best electrochemical properties. At 0.1*C* rate, its first specific discharge capacity is 159.7 mA·h/g in the voltage range of 2.75−4.30 V and 196.9 mA·h/g in the voltage range of 2.75−4.50 V; at 2*C* rate, its specific discharge capacity is 121.8 mA·h/g and still 119.7 mA·h/g after 40 cycles. The capacity retention ratio is 98.27%.

Key words: Li-ion batteries; cathode materials; $LiNi_{1/3}Co_{1/3}Mn_{1/3}O_2$; electrochemical performance

1 Introduction

Lithium cobalt oxide ($LiCoO_2$) is the most widely used commercial cathode material for lithium secondary batteries. However, the further application of $LiCoO_2$ was inhibited because of some drawbacks, such as high cost and toxicity of cobalt, instability of $LiCoO_2$ at high potential (above 4.2 V)[1−3]. Therefore, the extensive studies on alternatives to $LiCoO_2$ have been carried out in last decade[4−5]. For example, $LiNi_{1/3}Co_{1/3}Mn_{1/3}O_2$ was first proposed by OHZUKU and MAKIMURA[6] as a promising cathode material for Li-ion batteries in 2001. Due to the synergic effect, the outstanding electrochemical properties of $LiNi_{1/3}Co_{1/3}Mn_{1/3}O_2$ excelling those of $LiCoO_2$ or $LiNiO_2$ or $LiMnO_2$ were reported, and its reversible capacity was 160 mA·h/g in voltage range of 2.5−4.3V[7] or 200 mA·h/g in the voltage range 2.8−4.6 V[8]. In addition, excellent electrochemical performance at high discharge rate and outstanding thermal stability render $LiNi_{1/3}Co_{1/3}Mn_{1/3}O_2$ as one of the best candidates for the positive electrode material for hybrid electric vehicle power source systems[9]. Owing to its complicated composition, the electrochemical properties of $LiNi_{1/3}Co_{1/3}Mn_{1/3}O_2$ should be sensitively dependent on microscopic features like the distribution of transition metal, particle size and morphology. It is important to select a favorable synthetic method to obtain single phase and fine-sized powder. The liquid-phase co-precipitation method was usually adopted to prepare fine-sized precursor of nickel, cobalt, and manganese with desired particle morphologies and homogeneous transition metals distribution. The obtained precursor was mixed with LiOH and then sintered at certain temperature to prepare $LiNi_{1/3}Co_{1/3}Mn_{1/3}O_2$. The hydroxide co-precipitation method is one of the powerful methods[10−11]. However, the precipitated transition-metal hydroxide is easily oxidized in aqueous solution during the precipitation period. For example, $Mn(OH)_2$ is gradually oxidized to MnOOH or MnO_2, which can severely decrease the homogeneity of the final product. Thus, it is necessary to adopt feasible techniques to avoid Mn^{2+} oxidation in aqueous solution.

In this work, oxalic acid was used as a new effective precipitator in the co-precipitation method to prepare the precursor of $Ni_{1/3}Co_{1/3}Mn_{1/3}C_2O_4·2H_2O$. Due to the reducibility of the oxalic acid, the valence of manganese was always fixed at bivalence during precipitation period; consequently, the homogeneity of the precursor was effectively increased. And then the $LiNi_{1/3}Co_{1/3}Mn_{1/3}O_2$

Corresponding author: ZHANG Chuan-fu; Tel: +86-731-8830471; E-mail: cfzhang@mail.csu.edu.cn
DOI: 10.1016/S1003-6326(08)60325-8

powders were prepared by mixing the precursor and $LiOH·H_2O$(AR) by high-temperature calcination. The structures and morphologies of precursor and $LiNi_{1/3}Co_{1/3}Mn_{1/3}O_2$ were studied and the influence of sintering temperature on cathode material was also investigated.

2 Experimental

$NiCl_2·6H_2O$(AR), $CoCl_2·6H_2O$(AR), $MnCl_2·4H_2O$ (AR), and $H_2C_2O_4·H_2O$(AR) were used as raw materials. The mixed solution of metal (Ni, Co, Mn) chloride with total concentration of 0.6 mol/L was added drop by drop into reaction vessel containing oxalic acid solution used as precipitator, and the co-precipitation reaction was carried out at 30−85 ℃ with stirring speed of 500−850 r/min. In order to keep pH at a certain value, the calculated amount of alkaline solution was timely added into reaction vessel during co-precipitation period. A precipitation was obtained. To remove Cl^- in the sediment, the precipitation was filtered with distilled water again and again until Cl^- could not be detected by 1 mol/L $AgNO_3$ solution. After solid-liquid separation and distilled water washing, the sediment was dried at 105 ℃ in the vacuum drying cabinet. The content of transition metal, such as Ni, Co and Mn, in oxalate precursor, was determined by EDTA titration technique. The thermal behavior of obtained oxalate precursor in inert atmosphere in the temperature range of 25−1 000 ℃ was confirmed by TG-DTA analysis using the Japan CFS-Ⅱ thermal analyzer with the scan rate of 3 ℃/min.

The mixture of oxalate precursor and $LiOH·H_2O$ (AR) with stoichiometric ratio was ball milled by planet ball miller. After drying and screen separation, the mixture was sintered at 750−950 ℃ for a certain time to prepare $LiNi_{1/3}Co_{1/3}Mn_{1/3}O_2$.

The obtained $LiNi_{1/3}Co_{1/3}Mn_{1/3}O_2$ sample was characterized by X-ray diffraction meter (D/max-2400) with Cu K_α radiation. The system was equipped with a diffracted graphite mono-chromator. The morphology of the synthesized sample was observed by scanning electron microscope (SEM: JSM−5600LV, JEOF, Japan). The contents of metal elements, such as Li, Ni, Co and Mn, in obtained $LiNi_{1/3}Co_{1/3}Mn_{1/3}O_2$ powder, were determined by ICP-AES analyzer.

The cathodes for Li-ion cell were prepared by pressing the mixture of active material ($LiNi_{1/3}Co_{1/3}$-$Mn_{1/3}O_2$), conductive material (acetylene black) and binder(PVDF) with mass ratio of 85:10:5. After vacuum drying at 100 ℃ for 12 h, the electrode disks were punched and weighed. The cathodes were incorporated into cells with Li foil negative electrode, a Celgard separator and 1 mol/L $LiPF_6$ in EC:DMC (volume ratio 1:1) solvent. The cells were assembled in an argon-filled dry box. Constant charge-discharge tests were performed at room temperature in the voltage range of 2.75−4.50 V (vs Li/Li^+).

3 Results and discussion

3.1 Preparation of oxalate precursor

The morphology and crystal structure of obtained oxalate precursor are shown in Fig.1. The SEM image shows that the precursor is in polyhedral shape with particle size of about 10 μm, and the whole dispersion performance is well. The XRD pattern of the precursor demonstrates that all peaks are sharp and well-defined, suggesting that compound is well crystallized. Single-phase nickel oxalate, cobalt oxalate, or manganese oxalate is not found in XRD pattern, but its diffraction angle (2θ) and corresponding inter-planar distance(d) are consistent with those of monoclinic $FeC_2O_4·2H_2O$. It is indicated that stable oxalate compound with crystal structure similar to that of $FeC_2O_4·2H_2O$ is formed during the co-precipitation period. The results from chemical element analysis show that the contents of Ni, Co, and Mn in oxalate precursor are 10.39%, 10.90% and 9.85%, respectively. Consequently, the relative molecular mass of compound is calculated as 184.75, which is close to that of $Ni_{1/3}Co_{1/3}Mn_{1/3}C_2O_4·2H_2O$ (181.521 5). The DSC-TGA curves of precursor in inert gas in the temperature range of 25−1 000 ℃ are presented in Fig.2.

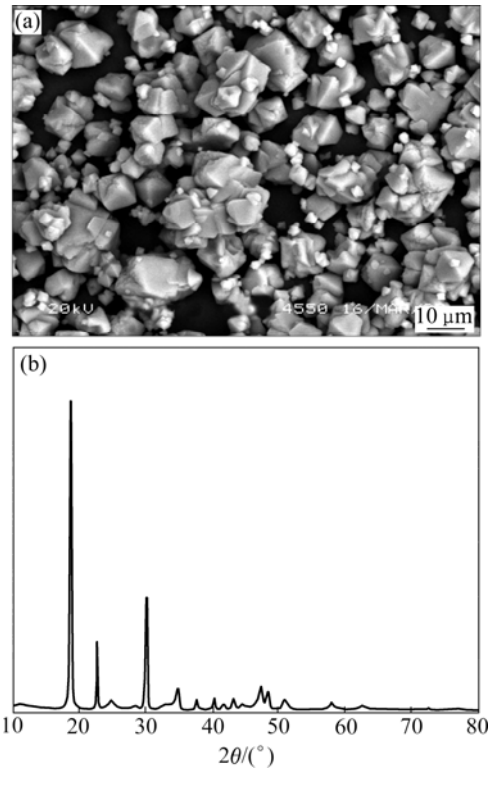

Fig.1 SEM image (a) and XRD pattern (b) of oxalate precursor

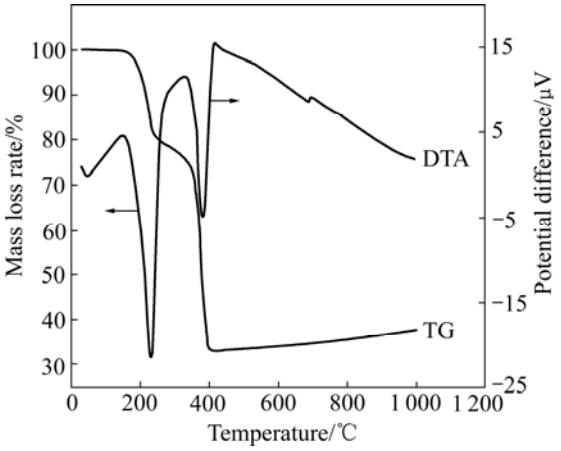

Fig.2 TG-DTA curves of oxalate precursor in inert gas

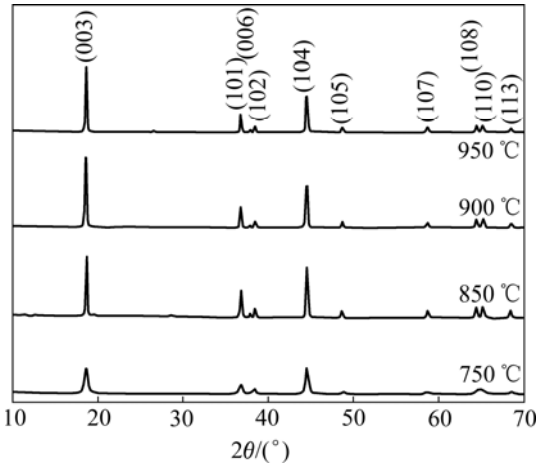

Fig.3 XRD patterns of $LiNi_{1/3}Co_{1/3}Mn_{1/3}O_2$ samples synthesized at different temperatures

The DTA profile has two aculeate endothermic peaks at 232.77 ℃ in the sector of 185.96−243.17 ℃ and at 381.76 ℃ in the sector of 353.10−407.58 ℃, while the corresponding TG curve shows apparent mass loss, 19.24% at 232.77 ℃ and 48.56% at 381.76 ℃, respectively. According to the following decomposition reactions (1) and (2),

$$Ni_{1/3}Co_{1/3}Mn_{1/3}C_2O_4\cdot 2H_2O = Ni_{1/3}Co_{1/3}Mn_{1/3}C_2O_4 + 2H_2O \quad (1)$$

$$Ni_{1/3}Co_{1/3}Mn_{1/3}C_2O_4 = Ni_{1/3}Co_{1/3}Mn_{1/3} + 2CO_2 \quad (2)$$

the corresponding theoretical mass loss rates of reactions (1) and (2) are 19.89% and 48.61%, respectively. Based on the results from XRD, chemical element analysis and TG-DTA, the molecular formula of obtained oxalate precursor can be determined as $Ni_{1/3}Co_{1/3}Mn_{1/3}C_2O_4\cdot 2H_2O$.

3.2 Synthesis of $LiNi_{1/3}Co_{1/3}Mn_{1/3}O_2$

3.2.1 Physical characterization of $LiNi_{1/3}Co_{1/3}Mn_{1/3}O_2$

The XRD patterns of $LiNi_{1/3}Co_{1/3}Mn_{1/3}O_2$ samples synthesized at different temperatures are illustrated in Fig.3. The diffraction peaks of obtained samples are quite similar to the results of YABUUCHI and OHZUKU[8]. It can be concluded that the $LiNi_{1/3}Co_{1/3}Mn_{1/3}O_2$ samples have α-$NaFeO_2$ layered structure (space group: $R3m$). No extraneous peak is found in the XRD pattern, indicating that the crystal phase is uniform and pure. In XRD patterns, the peak splits of (006)/(102) and (018)/(110) are known to be an indictor of layered structure like $LiCoO_2$ and $LiNiO_2$[12]. As shown in Fig.3, clear peak splits of (006)/(102) and (018)/(110) are observed when temperature is higher than 750 ℃, therefore, the obtained $LiNi_{1/3}Co_{1/3}Mn_{1/3}O_2$ sample has a highly ordered layered structure.

In hexagonal unit cell, the lattice parameter a is related to average metal-metal intras-lab distance, while the lattice parameter c is related to the average metal-metal inters-lab distance[13]. For layered compounds, a higher value of c/a is desirable for better hexagonal structure [14]. The lattice parameters a, c, and c/a of $LiNi_{1/3}Co_{1/3}Mn_{1/3}O_2$ sample synthesized at different temperatures are listed in Table 1. As shown in Table 1, the value of c/a, which increases with the elevation of sintering temperature, for $LiNi_{1/3}Co_{1/3}Mn_{1/3}O_2$ sample synthesized in the temperature range of 750−950 ℃, is as high as 4.97. So, the obtained sample has a well-defined hexagonal structure. On the other hand, cation mixing in layered structure oxides can deteriorate its electrochemical performance[15−16]. The intensity ratios of I_{003}/I_{104} (R) and $(I_{102}+I_{006})/I_{101}$($R'$) are sensitive to the degree of cation mixing in lattice[17−18]. Therefore, R and R' are often used to measure the degree of the cation mixing. Higher value of R and lower value of R' are desirable for a lower degree of the cation mixing. $R<1.2$ is an indication of undesirable cation mixing. The values of R and R' for $LiNi_{1/3}Co_{1/3}Mn_{1/3}O_2$ samples synthesized at different temperatures are presented in Table 1. It is manifested that R increases accordingly from 1.00 to 1.66 when the sintering temperature is elevated from 750℃ to 900 ℃, while R' decreases consequently from 0.46 to 0.39. However, R begins to debase and R' to ascend when the sintering temperature is higher than 900℃. Therefore, appropriate temperature is the key factor for the lower degree of cation mixing in lattice. The $LiNi_{1/3}Co_{1/3}Mn_{1/3}O_2$ sample synthesized at 900 ℃ has a well-defined hexagonal structure, and the degree of cation mixing is lower, indicating that its electrochemical properties is better.

The morphologies of the $LiNi_{1/3}Co_{1/3}Mn_{1/3}O_2$ sample synthesized at different temperatures were observed with scanning electron microscope (Fig.4). The particles are in irregular shape, and most of them are flaky

Table 1 Lattice parameters and I_{003}/I_{104} and $(I_{006}+I_{102})/I_{101}$ of $LiNi_{1/3}Co_{1/3}Mn_{1/3}O_2$ samples synthesized at different temperatures

Synthesis temperature/℃	I_{003}	I_{003}/I_{104}	$(I_{006}+I_{102})/I_{101}$	a/Å	c/Å	c/a
750	1716	1.00	0.46	2.860 74	14.205 51	4.965 7
850	3480	1.06	0.43	2.861 09	14.219 15	4.969 8
900	4522	1.66	0.39	2.861 32	14.222 98	4.970 8
950	4718	1.65	0.44	2.861 37	14.231 15	4.973 5

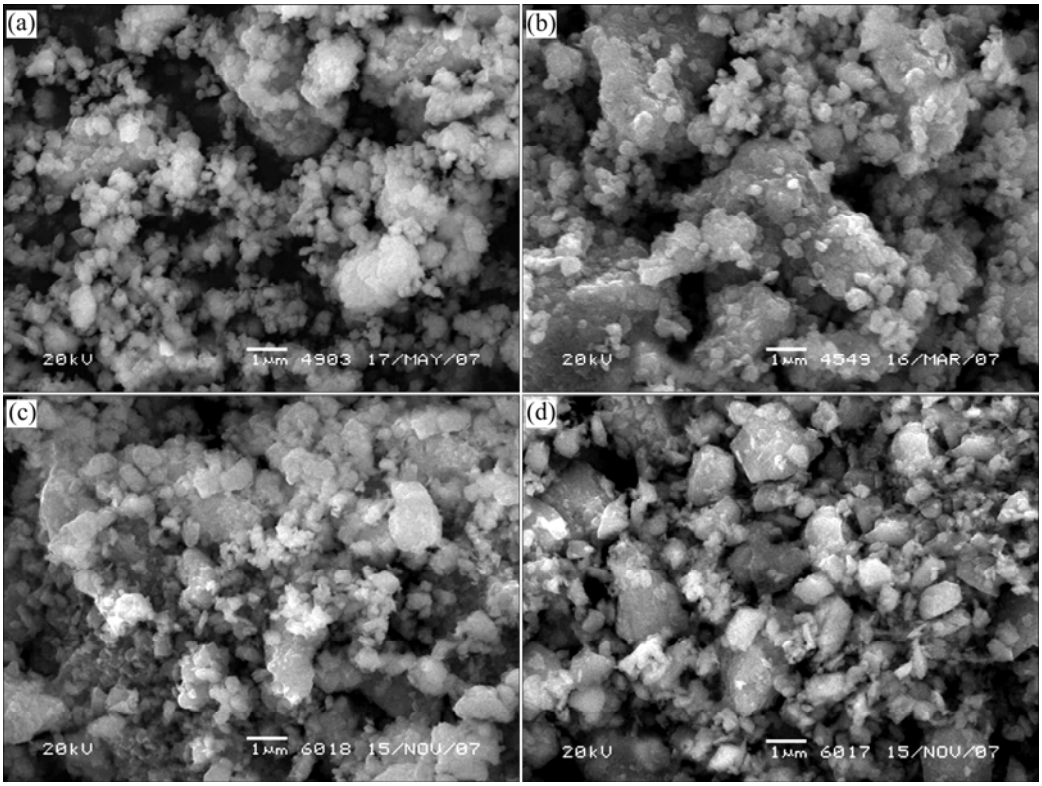

Fig.4 SEM images of $LiNi_{1/3}Co_{1/3}Mn_{1/3}O_2$ samples synthesized at different temperatures: (a) 750 ℃; (b) 850 ℃; (c) 900 ℃; (d) 950 ℃

or homo-spherical with particle size of 200−500 nm. In addition, the particle size of sample synthesized at 950 ℃ is apparently larger than that of sample synthesized at 750 ℃. The aggregation of particle is enhanced with the elevation of sintering temperature, and the porosity of sample is obviously decreased.

As mentioned above, the content and the distribution of nickel, cobalt, manganese in obtained sample have great influences on the electrochemical performance of $LiNi_{1/3}Co_{1/3}Mn_{1/3}O_2$. To ensure better electrochemical properties, stoichiometrical ratio and homogeneous distribution of Ni, Co and Mn in $LiNi_{1/3}Co_{1/3}Mn_{1/3}O_2$ sample are indispensable. Based on the ICP-AES analysis result, the contents of Li, Ni, Co and Mn in the sample are 7.21%, 19.11%, 20.15% and 18.21%, respectively, and their molar ratio is n(Li):n(Ni):n(Co):n(Mn)=3.09:0.975:1.026:0.993, which is close to the theoretical value (n(Li):n(Ni):n(Co):n(Mn)=3:1:1:1). The distribution of Ni, Co and Mn in the sample was confirmed by EDX analysis, as presented in Fig.5.

Through micro-zone scanning on random area, it is indicated that the distribution of Ni, Co and Mn is homogeneous and their molar ratio is close to 1:1:1. The possible reason for minim quantity of element silicon observed in Fig.5 may be the dust brought during the experimental operation. Based on the results from ICP-AES and EDX analysis, it can be concluded that Ni^{2+}, Co^{2+} and Mn^{2+} in reaction solution are co-precipitated by oxalic acid with stoichiometric ratio during liquid-phase co-precipitation process, and the difference between practical composition of $LiNi_{1/3}Co_{1/3}Mn_{1/3}O_2$ sample and its theoretical value is minimized. The possible reasons for these phenomena may be as follows: firstly, using oxalic acid as precipitator, Ni^{2+}, Co^{2+} and Ni^{2+} begin to precipitate at a similar pH value due to complex reaction with oxalic ion; furthermore, the oxidation of Mn^{2+} during the co-precipitation process without inert gas protection can be avoided effectively because of oxalic acid reducibility, and impurities such as MnOOH and MnO_2 are not found in oxalate precursor. As a result, using oxalate precursor

and $LiOH·H_2O$ as starting material, the distribution of Ni, Co and Mn in $LiNi_{1/3}Co_{1/3}Mn_{1/3}O_2$ sample synthesized with solid-phase reaction method is homogeneous, and their molar ratio is close to stoichiometric value.

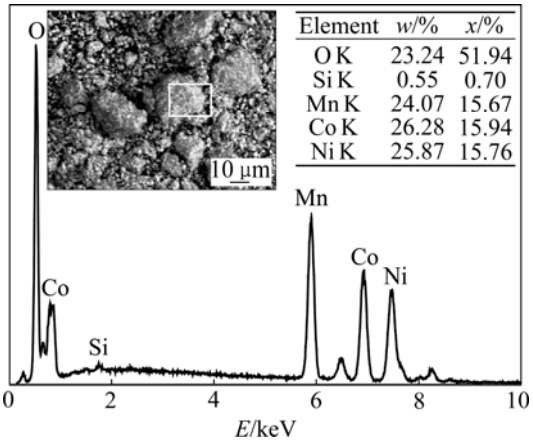

Fig.5 EDX analysis of $LiNi_{1/3}Co_{1/3}Mn_{1/3}O_2$ sample

3.2.2 Electrochemical performance of $LiNi_{1/3}Co_{1/3}Mn_{1/3}O_2$

The initial charge/discharge curves of $LiNi_{1/3}Co_{1/3}Mn_{1/3}O_2$ samples synthesized at different temperatures are plotted in Fig.6. As seen in Fig.6, all samples show good charge-discharge performance at the current density of 0.1*C* in the voltage range of 2.75−4.30 V. A steady charge-discharge plateau and a long constant current duration are observed in charge-discharge period. Moreover, the mid-value voltage is as high as 3.72 V. But the initial charge/discharge capacity of sample is variable with sintering temperature. The $LiNi_{1/3}Co_{1/3}Mn_{1/3}O_2$ synthesized at 900℃ has the highest charge/discharge capacity of 185.3/159.7 mA·h/g. These phenomena can be explained by the effect of sintering temperature on the crystal structure and micro-morphology of $LiNi_{1/3}Co_{1/3}Mn_{1/3}O_2$ sample[15−16]. As mentioned above, the crystal growth is complete and the degree of cation mixing in lattice also decreases with the elevation of sintering temperature. Consequently, the $LiNi_{1/3}Co_{1/3}Mn_{1/3}O_2$ sample with well-fined hexagonal structure and best electrochemical properties is obtained at a higher temperature. However, when the sintering temperature is higher than 900 ℃, the particle size of sample increases remarkably, and the degree of cation mixing in crystal lattice is dramatically enhanced too. As a result, the initial charge/discharge capacity of $LiNi_{1/3}Co_{1/3}Mn_{1/3}O_2$ sample synthesized at 950 ℃ decreases to 166.9/145.2 mA·h/g.

First charge/discharge curves of $LiNi_{1/3}Co_{1/3}Mn_{1/3}O_2$ sample synthesized at 900 ℃ under different charge-end voltages are shown in Fig.7, and its cycle performance under different charge/discharge rates are presented in Fig.8. As shown in Fig.7, the charge/discharge capacity increases accordingly from 185.3/159.7 mA·h/g to 230.5/196.9 mA·h/g when the charge-end voltage enhances from 4.3 V to 4.5 V. The charge/discharge capacity increases continuously to its theoretical value (270 mA·h/g) with the elevation of

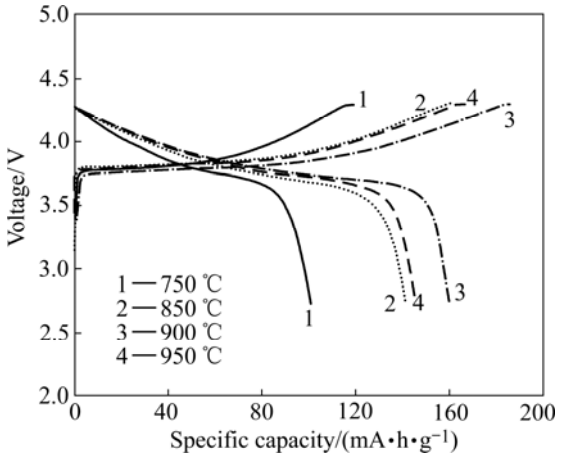

Fig.6 First charge/discharge curves of $LiNi_{1/3}Co_{1/3}Mn_{1/3}O_2$ samples synthesized at different temperatures under 0.1*C*

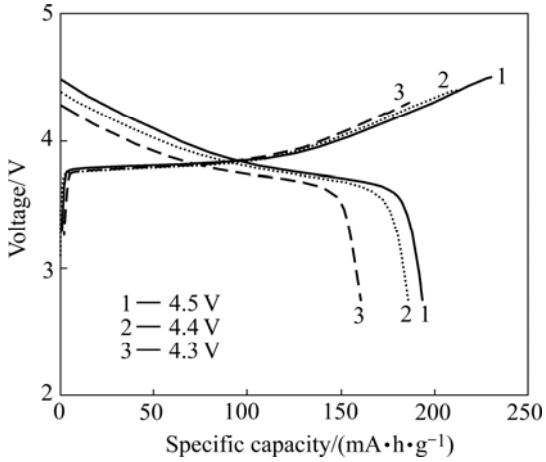

Fig.7 First charge/discharge curves of $LiNi_{1/3}Co_{1/3}Mn_{1/3}O_2$ sample synthesized at 900 ℃ under different charge-end voltages

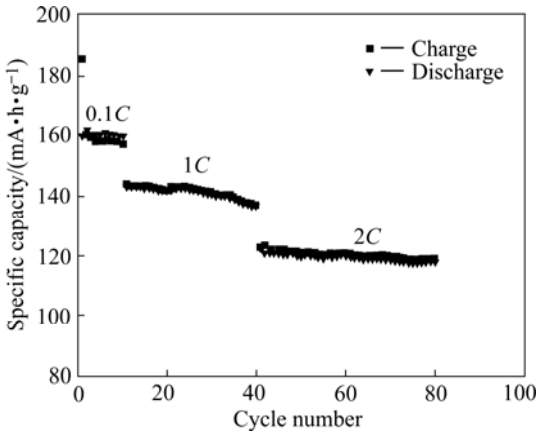

Fig.8 Cycle performances of $LiNi_{1/3}Co_{1/3}Mn_{1/3}O_2$ sample synthesized at 900 ℃ under different charge-discharge rates

charge-end voltage. According to the principle of chemical reaction, more Li^+ can pull out and more Ni^{2+} and Co^{2+} can be oxidized with the increasing of charge-end voltage. As a result, the electrochemistry reaction is endlessly impelled to complete, and charge capacity increases consequently. Compared with $LiCoO_2$, the charge/discharge of $LiNi_{1/3}Co_{1/3}Mn_{1/3}O_2$ can be conducted at higher charge-end voltage, and thus more energy is provided. Presently, the practical specific capacity of $LiCoO_2$ in application is about 145 mA·h/g by charging up to 4.2 V, and about 50% of Li^+ takes effect in charge/discharge reaction. Extracting more Li^+ from $LiCoO_2$ lattice can dramatically decrease its lattice parameter *c* through phase transition from hexagonal to monoclinic, and the crystal structure collapses finally [19]. But former phase transition can be suppressed owing to Mn^{4+} in $LiNi_{1/3}Co_{1/3}Mn_{1/3}O_2$. It is also indicated in Fig.7 that charge capacity of $LiNi_{1/3}Co_{1/3}Mn_{1/3}O_2$ sample is higher than its discharge capacity, and the coulomb efficiencies under different charge-end voltages are as follows: 86.18% (4.5 V), 87.30% (4.4 V), and 85.40% (4.3 V). The reasons for irreversible capacity occurred in the initial charge/discharge process are the cation mixing and Li^+ consumption due to SEI membrane formed on anode material[20]. The irreversible capacity of $LiNi_{1/3}Co_{1/3}Mn_{1/3}O_2$ is large in the first charge/discharge cycle, but charge capacity is close to discharge capacity since the second cycle, as shown in Fig.8.

High energy and large power are the development trend of new generation of lithium-ion battery, especially in the aspect of vehicle power source, which requires larger specific capacity and excellent cycling performance at higher charge/discharge rate. As presented in Fig.8, the specific capacity of $LiNi_{1/3}Co_{1/3}Mn_{1/3}O_2$ decreases from 160 mA·h/g to 120 mA·h/g when the charge-discharge rate increases from 0.1*C* to 2*C*. The specific capacity of obtained sample is higher under smaller current density and lower charge/discharge rate. On the other hand, Fig.8 also reveals that the charge/discharge curve is almost on a line at a same rate, which means that coulomb efficiency is high and $LiNi_{1/3}Co_{1/3}Mn_{1/3}O_2$ sample has excellent cycling performance. For example, at 2*C* rate, the discharge specific capacity of obtained sample is 121.8 mA·h/g in the 41st cycle and it still retains as 119.7 mA·h/g in the 80th cycle. The capacity retention ratio is 98.27% after 40 cycle. The results mentioned above demonstrate that $LiNi_{1/3}Co_{1/3}Mn_{1/3}O_2$ synthesized from oxalate precursor has larger capacity and excellent cycling performance at higher charge/discharge rate, which is sufficient to the demands of power supply of electric vehicle.

4 Conclusions

1) Owning to oxalic acid reducibility and complex reaction among Ni^{2+}, Co^{2+}, Mn^{2+} and oxalic ions, the $Ni_{1/3}Co_{1/3}Mn_{1/3}C_2O_4{\cdot}2H_2O$ precursor with stoichiometric ratio and homogeneous distribution of transition metals is obtained by liquid-phase co-precipitation method.

2) By using $Ni_{1/3}Co_{1/3}Mn_{1/3}C_2O_4{\cdot}2H_2O$ precursor and $LiOH{\cdot}H_2O$ as starting materials, the $LiNi_{1/3}Co_{1/3}Mn_{1/3}O_2$ cathode material was synthesized by solid-state reaction method. Sintering temperature has remarkable influence on the crystal structure and micro-morphology of obtained sample. The $LiNi_{1/3}Co_{1/3}Mn_{1/3}O_2$ synthesized at 900 ℃ has desirable particle size and well-defined *a*-$NaFeO_2$ layered structure with a lower degree of cation mixing.

3) The $LiNi_{1/3}Co_{1/3}Mn_{1/3}O_2$ synthesized at 900 ℃ has the best electrochemical properties. At 0.1*C* rate, its first specific discharge capacity is 159.7 mA·h/g (2.75−4.30 V) and 196.9 mA·h/g (2.75−4.50 V), respectively. At 2*C* rate, its specific discharge capacity is 121.8 mA·h/g and still retains as 119.7 mA·h/g after 40 cycles. The capacity retention ratio is 98.27%. The results demonstrate that $LiNi_{1/3}Co_{1/3}Mn_{1/3}O_2$ synthesized from oxalate precursor has larger capacity and excellent cycling performance at higher charge/discharge rate, which is sufficient to the demands of power supply of electric vehicle.

References

[1] KOKSBANG R, BARKER J, SHI H, SAIDI M Y. Cathode materials for lithium rocking chair batteries [J]. Solid State Ionics, 1996, 84: 1−21.

[2] MACNEIL D D. An autocatalytic mechanism for the reaction of Li_xCoO_2 in electrolyte at elevated temperature [J]. J Electrochem Soc, 2000, 147(3): 970−979.

[3] PENG Z S, WAN C R, JIANG C Y. Synthesis by sol-gel process and characterization of $LiCoO_2$ cathode materials [J]. J Power Sources, 1998, 72(2): 215−220.

[4] CHEN Y, WANG G X, KONSTANTINOV K, LIU H K, DOU S X. Synthesis and characterization of $LiCo_xMn_yNi_{1-x-y}O_2$ as a cathode material for secondary lithium batteries [J]. J Power Sources, 2003, 119/121: 184−188.

[5] LIU Z, YU A, LEE J Y. Synthesis and characterization of $LiNi_{1-x-y}Co_xMn_yO_2$ as the cathode materials of secondary lithium batteries [J]. J Power Sources, 1999, 81/82: 416−419.

[6] OHZUKU T, MAKIMURA Y. Layered lithium insertion material of $LiCo_{1/3}Ni_{1/3}Mn_{1/3}O_2$ for lithium-ion batteries [J]. Chem Lett, 2001(7): 642−643.

[7] SHAJU K M, SUBBA RAO G V, CHOWDARI B V R. Performance of layered $Li(Ni_{1/3}Co_{1/3}Mn_{1/3})O_2$ as cathode for Li-ion batteries [J]. Electrochimica Acta, 2002, 48(2): 145−151.

[8] YABUUCHI N, OHZUKU T. Novel lithium insertion material of

$LiCo_{1/3}Ni_{1/3}Mn_{1/3}O_2$ for advanced lithium-ion batteries [J]. J Power Sources, 2003, 119/121(1/2): 171−174.

[9] BELHAROUAK I, SUN Y K, LIU J, AMINE K. $Li(Co_{1/3}Ni_{1/3}Mn_{1/3})O_2$ as a suitable cathode for high power applications [J]. J Power Source, 2003, 123(2): 247−252.

[10] MIJUNG N, LEE Y, CHO J. Water adsorption and storage characteristics of optimized $LiCoO_2$ and $LiNi_{1/3}Co_{1/3}Mn_{1/3}O_2$ composite cathode material for Li-ion cells [J]. J Electrochem Soc, 2006, 153(5): 935−940.

[11] CHOI J, MANTHIRAM A. Investigation of the irreversible capacity loss in the layered $LiCo_{1/3}Ni_{1/3}Mn_{1/3}O_2$ cathodes [J]. Electrochemical and Solid-State Letters, 2005, 8(8): C102−105.

[12] CHO J, KIM G, LIM H S. Effect of preparation methods of $LiNi_{1-x}Co_xO_2$ cathode materials on their chemical structure and electrode performance [J]. J Electrochem Soc, 1999, 146(10): 3571−3576.

[13] LUO X F, WANG X Y, LIAO L, WANG X M. Effects of synthesis conditions on the structural and electrochemical properties of layered $Li[Ni_{1/3}Co_{1/3}Mn_{1/3}]O_2$ cathode material via the hydroxide co-precipitation method LIB SCITECH [J]. J Power Sources, 2006, 161: 601−605.

[14] REIMERS J N, ROSSEN E, JONES C D, DAHA J R. Structure and electrochemistry of $Li_xFe_yNi_{1-y}O_2$ [J]. Solid State Ionics, 1993, 61(4): 335−344.

[15] KYUNG K L. Electrochemical and structure characterization in $LiNi_{1-y}Co_yO_2(0\leqslant y\leqslant 0.2)$ position electrodes during initial cycling [J]. J Electrochem Soc, 2000, 147(5): 1715−1723.

[16] PERES J P, DELMAS C, ROUGIER A, BROUSSELY M, PERTON F, BIENSAN P, WILLMANN P. The relationship between the composition of lithium nickel oxide and the loss of reversibility during the first cycle [J]. J Physics and Chemistry of Solids, 1996, 57(6/8): 1057−1060.

[17] LIU Z L, AISHUI Y, LEE J Y. Modifications of synthetic graphite for secondary lithium-ion battery application [J]. J Power Sources, 1999, 81/82: 187−191.

[18] DAHN J R, SACKEN U, MICHAL A. Structure and electrochemistry of $Li_{1\pm y}NiO_2$ and a new Li_2NiO_2 phase with the $Ni(OH)_2$ structure [J]. Solid State Ionics, 1990, 44(1/2): 87−97.

[19] KOBAYASHI H, ARACHI Y, EMURA S, KAGEYAMA H, TATUSMI K, KAMIYAMA T. Investigation on lithium de-intercalation mechanism for $Li_{1-y}Ni_{1/3}Mn_{1/3}Co_{1/3}O_2$ [J]. J Power Sources, 2005, 146: 640−644.

[20] MEGAHED S, SCROSATI B. Lithium-ion rechargeable batteries [J]. J Power Sources, 1994, 51(1/2): 79−104.

(Edited by YANG Hua)